A novel energy reconstruction for high-energy gamma-ray wide field of view observatories

Laura Beatriz da Rocha Zink Fernandes Peres
Instituto Superior Técnico, Lisboa, Portugal
(Dated: 29th November 2021)

A novel method to reconstruct the slant depth of the maximum of the longitudinal profile of high-energy showers initiated by gamma-rays, $X_{\max}$, as well as their energy, E_0 is presented. The method was developed for gamma-rays with energies ranging from a few hundred GeV to ~ 10 TeV.

Event-by-event, an estimator of $X_{\max}$ is obtained from its correlation with the distribution of the arrival time of the particles at the ground, or the signal at the ground for lower energies. An estimator of E_0 is obtained, event-by-event, using a parametrization that has as inputs the total measured energy at the ground, the amount of energy contained in a region near to the shower core and the estimated $X_{\max}$.

Resolutions of about 40 (20) g/cm^2 and about 30 (20)% for, respectively, $X_{\max}$ and E_0 at 1 (10) TeV energies are obtained, considering vertical showers. The obtained results are promising and may pave the way for the development of novel physics possibilities for large wide-field-of-view gamma-ray observatories.

Keywords: High Energy gamma-rays; Wide field observatories; Depth of the shower maximum; Energy distribution at the ground; Primary energy reconstruction resolution.

I. INTRODUCTION

Some of the fundamental questions in astroparticle physics right now are around the high-energy particles that arrive from space. Despite being but a small fraction of the flux of cosmic rays, gamma-rays are the ideal messenger particle of the relativistic universe due to their unique properties.

They are neutral particles, which means that they cannot be deflected in their journey through space by galactic and extragalactic magnetic fields, and so they can directly be back-traced to their point of origin. This means that gamma-ray detection is a particularly important topic that could tell us a great deal about gamma-ray sources and the nature of cosmic rays. The ultimate nature of matter and physics beyond the Standard Model may also have a clue in the spectrum of very-high energy (VHE) gamma-rays, since high-energy gamma-ray astrophysics is sensitive to energy scales important for particle physics. The answer to these fundamental questions, as it often happens in physics, hinges on the development of better detection techniques.

The direct detection of primary gamma-rays is only possible with satellite-based detectors because the atmosphere is opaque to high-energy gamma-rays. The detection with ground-based instruments is done via the Extensive Air Showers (EAS) that are created when a gamma-ray interacts with the atmosphere. When a gamma-ray enters the atmosphere, it generates a cascade of secondary particles: the first photon converts into a pair of e^+ e^- at high altitudes, and each of them radiate a secondary gamma-ray, mostly through bremsstrahlung, which also converts into a pair e^+ e^- of lower energies. This repeats several times until eventually, the electron-positron pairs will reach the critical energy, where the shower has the maximum number of particles and after which it diminishes. The atmospheric depth for the shower maximum is labelled $X_{\max}$, which can be related to the stage at which the shower reaches the ground.

Extensive Air Showers may be characterised by the distributions of the number of shower particles N as a function of the traversed atmospheric slant depth X, the longitudinal profile; and/or by the distributions of the particles arriving at the ground level as a function of the distance to the shower core, the Lateral Density Function (LDF).

The longitudinal development of gamma-ray initiated showers was historically described by Rossi and Greisen diffusion equations [1] being the well known Greisen [2] and Gaisser-Hillas [3] functions approximate solutions. It can be demonstrated that these functions lead to a quasi-universal shape [4]. This universality can be shown by representing the shower longitudinal profile in the plane ($N' = N/N_{\max}$, $X' = X - X_{\max}$), where $X_{\max}$ is the slant depth of the maximum of the profile and $N_{\max}$ is the number of the shower particles at that depth. In this reference frame, the profile may be seen as a slightly asymmetric Gaussian with variable width and is essentially insensitive to variations induced by the depth of the first interaction [5]. However, at TeV energies or below, the fraction of events where the longitudinal profile does not follow the quasi-Gaussian shape may not be negligible. A few of the profiles will have a slower decrease after the $X_{\max}$ or even having a double peak structure. These anomalous shower profile structures are associated with interactions where particles travel several radiation/interaction lengths before interacting, or when one of the sub-products of the interaction takes nearly all the available energy.

The ground-based gamma-ray experiments can detect VHE gamma-rays in two ways, Imaging Cherenkov Telescopes (IACTs) and EAS arrays.

The Cherenkov light produced by the EAS is collected by the IACT, which can reconstruct the energy and the direction of the primary gamma-ray using the size, intensity and orientation of the projected image in the camera focal plane.

EAS arrays work by observing the secondary particles, mainly electrons and photons, of the EAS as they reach the ground. The shower core position and the direction of the primary gamma-ray are determined with acceptable accuracy by the arrival time and position distributions. However, the determination of the shower energy has a large uncertainty. Energy resolutions of the order of several tens of percent are often quoted for TeV showers. The main issue for the energy reconstruction remains in the uncertainty on the position of the first interaction in the atmosphere. Contrary to IACT arrays, there is no direct measurement for ground arrays of the contents of the EAS in the region of the shower maximum, and therefore the shower development stage is unknown.

The easiest way to obtain an estimate for the gamma-ray primary energy with an EAS array is to count the number of detector elements triggered by the EAS. It has been used by a variety of experiments [6] but, it does not consider important aspects of the event such as the zenith angle, the location of the shower core or its containment within the array. The shower containment, in particular, can have an unfavourable impact, since higher energies events can trigger all the detector elements and thus have an impossible estimation. All this means that just the fraction of detector elements hit is a weak estimation for the primary energy. The application of this method by the HAWC collaboration recently obtained a resolution of about 55% for 10 TeV events; HAWC has also tested a new algorithm for the reconstructing the energies of gamma-ray events using a neural network and a resolution of around 40% for 10 TeV events is obtained [7].

For showers induced by gamma-rays, with the same energy and zenith angle, the number of particles at the ground is expected to increase with $X_{\max}$. This is not universal, because the width of the longitudinal profile is also a significant factor in determining not only the total energy at the ground, but also the fraction of that energy present in the shower core region. For the same $X_{\max}$, a larger shower profile width will have more energy at the ground and a larger fraction of energy in the region around the core. It is then possible to establish, at fixed primary energy, a correlation between the fraction of the energy in the region near the core and the total energy carried by electromagnetic particles (photons, electrons and positrons) that reach the ground (S_{em}).

In this work we propose a new method to improve the determination of the primary energy by using the electromagnetic energy at the ground, S_{em}, and estimate the shower development stage using either S_{em} or at higher energies the curvature of the shower front. We also show that it is necessary to correct for anomalous shower development and that such can be achieved using the ratio of electromagnetic energy near the shower core (up to 20 meters) with respect to S_{em}.

All the present results were obtained using CORSIKA (version 7.5600) [8] to simulate vertical gamma-ray showers assuming an observatory at an altitude of 5200 m a.s.l. The gamma-rays, with energies between 250 GeV and 15 TeV, were injected following an energy spectrum of E^{-1}, which guarantees high enough statistics over the whole simulated energy range. It was used as a hadronic interaction model for low and high energy, FLUKA [9, 10] and QGSJET-II.04 [11], respectively, although the choice of these models has little impact on the simulation of electromagnetic showers. The total energy of electromagnetic shower particles was recorded at the observation level and histogrammed in radial bins of 4 meters. This would mimic a calorimeter detector compact array, where the station unit covers an area of $\sim 12\,\mathrm{m}^2$.

II. CONCEPT OF THE NOVEL RECONSTRUCTION METHOD

We can illustrate how the core of this work, the new reconstruction method, will be developed. We will establish two different energy reconstructions and in both cases we start with E_0 that needs to be estimated. In Figure 1 we have a schematic representing the steps needed to obtain the reconstructions.

On the left, in green, we see the steps needed to take to obtain the 0-order reconstruction, that will be seen at the start of section V. We only use one of the shower characteristics, the energy at the ground, S_{em}. In section III we will determine a corresponding estimator for this observable, A_0, that can be used for the reconstruction. Then a simple power-law will establish the parametrization of our first energy reconstruction.

For the novel energy reconstruction method, besides S_{em}, we will use more of the shower characteristics, to create a more robust estimation. As we can see on the orange diagram of Figure 1, they will be the anomalous development of a shower and $X_{\max}$. To estimate the anomalous development, we will create a new variable, f_{20}, related to the amount of energy near the shower core, that serves as an extrapolation of the behaviour of the shower on the air, which can be seen in more detail in section III. In section IV it is explained how we can use two different ways of estimating $X_{\max}$, from the shower curvature at the ground and the energy at the ground. Finally, in section V, all these puzzle pieces will be joined, and we will obtain a new energy parametrization that has as inputs the total measured energy at the ground, the amount of energy contained in a region near to the shower core and the estimated $X_{\max}$.

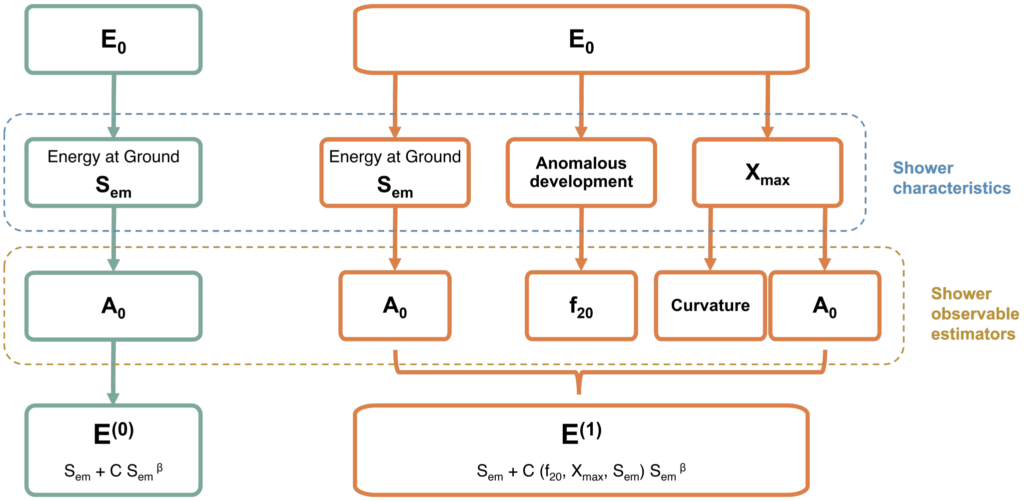

Figure 1. Schematic of the components needed for the two energy reconstruction methods that are used in this work. The green diagram represents the 0-order energy reconstruction. In the orange diagram we have the constituents of the novel energy reconstruction strategy. In the blue dotted box are the shower characteristics that are necessary for each method, while in the yellow dotted box we have their respective shower observable estimators.

III. ENERGY DISTRIBUTION AT THE GROUND

The goal of this work is to characterize the shower development through a method that takes into account the shower stage using two variables, which will be then used to predict, event by event, the calibration factor between the gamma-ray energy (E_0) and the electromagnetic energy arriving at the ground ($S_{\rm em}$).

One of these variables is clearly $X_{\rm max}$, which serves as a proxy to the shower stage. The other is defined as the ratio between the energy at the ground collected at a distance less than 20 m from the shower core and the total energy at the ground, f_{20}. For a given E_0 and $X_{\rm max}$, the development of the shower between the $X_{\rm max}$ region and the ground level will effectively determine f_{20}. This parameter will be the key element in the improvement of the energy resolution achieved in this work.

The energy distribution at the ground as a function of the distance r to the core position and its cumulative function, $F(r)$, are shown in Figure 2 for an event with $S_{\rm em} = 96.5\,{\rm GeV}$, $E_0 = 1165.9\,{\rm GeV}$ and $X_{\rm max} = 334\ {\rm g\,cm^{-2}}$.

We need to build an estimator of $S_{\rm em}$, defined as A_0, which can be obtained by the correlation between $S_{\rm em}$ and $F_{r_0} \equiv F(r_0)$, being r_0 a reference distance. The optimal choice for r_0 should be greater than 20 m to ensure a good correlation, and lower than some tens of meters to ensure a high number of events where the event footprint, with $r < r_0$, is fully contained within the compact array region of the observatory. In this work $r_0 = 50\,{\rm m}$ was chosen.

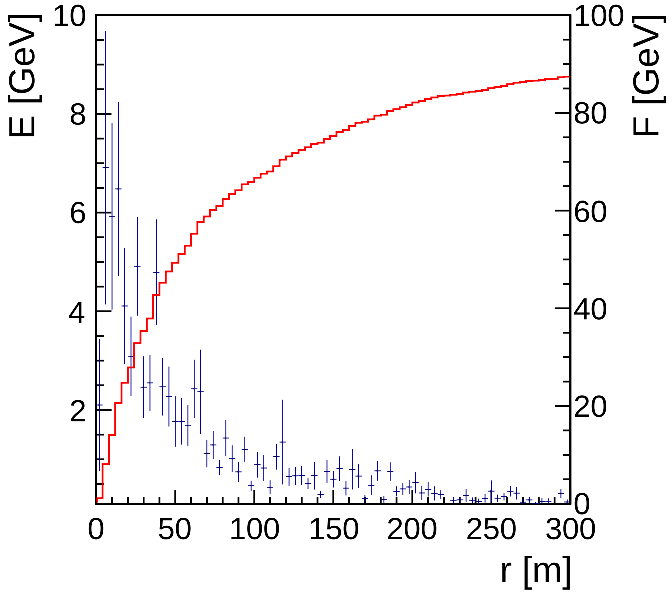

Figure 2. The energy distribution at the ground for one event with $S_{\rm em} = 96.5\,{\rm GeV}$, $E_0 = 1165.9\,{\rm GeV}$ and $X_{\rm max} = 334\ {\rm g\,cm^{-2}}$. Also shown the respective cumulative function $F(r)$.

The correlation between $S_{\rm em}$ and F_{50} is shown in Figure 3 and A_0 is parametrized as:

$$A_0 = F_{50} + G\,F_{50}^{\delta} \tag{1}$$

where G and δ are free positive parameters. The best parametrization is shown as the red curve in Figure 3, corresponding to $G = 1.63\,{\rm GeV}^{0.28}$ and $\delta = 0.72$.

The obtained resolutions and bias[12] of A_0 are summarized in Figure 4, as a function of $S_{\rm em}$. A primary

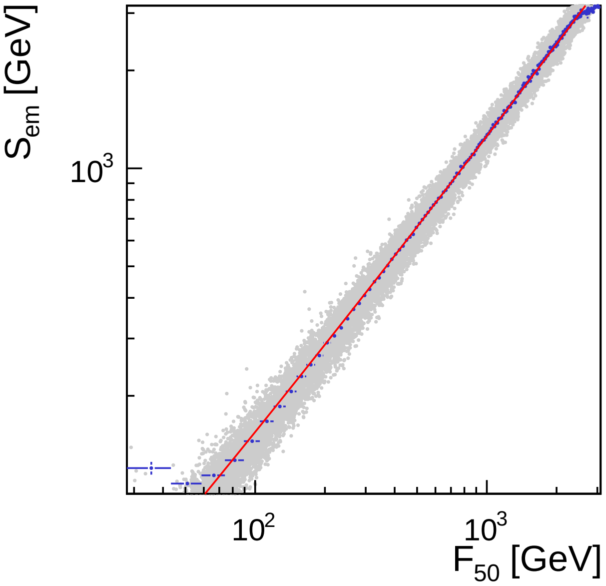

Figure 3. Correlation between the electromagnetic energy deposited at the ground, $S_{\rm em}$, and F_{50}, the energy deposited at the ground within a radius of 50 m from the core position.

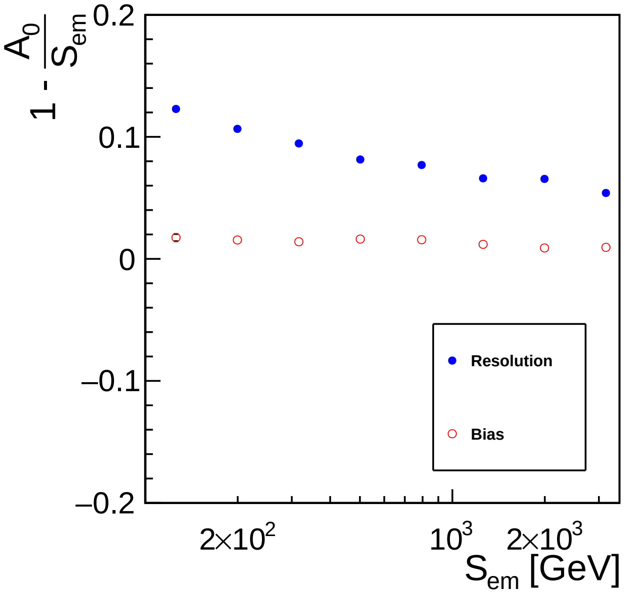

Figure 4. Bias and the relative resolution of the estimator of the energy deposited at the ground, A_0, as a function of the energy deposited at the ground, $S_{\rm em}$.

energy of 1 TeV and 10 TeV corresponds to a mean value of $S_{\rm em}$ of 115 GeV and 3 TeV, respectively (see Figure 10). This means that resolutions of about 12% and 5% are found at primaries energies of 1 TeV and 10 TeV, respectively, while the bias is consistently in the order of a few percent.

We can now define f_{20} as F_{20}/A_0. In this work, the reference value of 20 m for the definition of this variable was chosen, but it is a compromise that should be optimized for each specific experiment. Even so, its value should largely be between 15 m and 30 m. Values lower than that will conflict with the possible experimental resolutions on the shower core, while higher values will enter the region where the cumulative function has a slower increase and where, for events with the core nearer to the border of the compact region of the array, there will be no direct measurement of the cumulative function.

IV. $X_{\rm max}$ RECONSTRUCTION AND RESOLUTION

An easy first-order estimation of $X_{\rm max}$ can be obtained by the relation that $X_{\rm max}$ has with the electromagnetic energy that reaches the ground, $S_{\rm em}$, reflecting the increase of the shower size with the primary energy. This correlation is demonstrated in Figure 5 where $X_{\rm max}$ is represented as a function of $S_{\rm em}$. It is then possible to parametrize $X_{\rm max}$ as a function of $S_{\rm em}$ as:

$$X^0_{\rm max} = B_0 + \gamma_0 \log(S_{\rm em}/{\rm GeV}), \qquad (2)$$

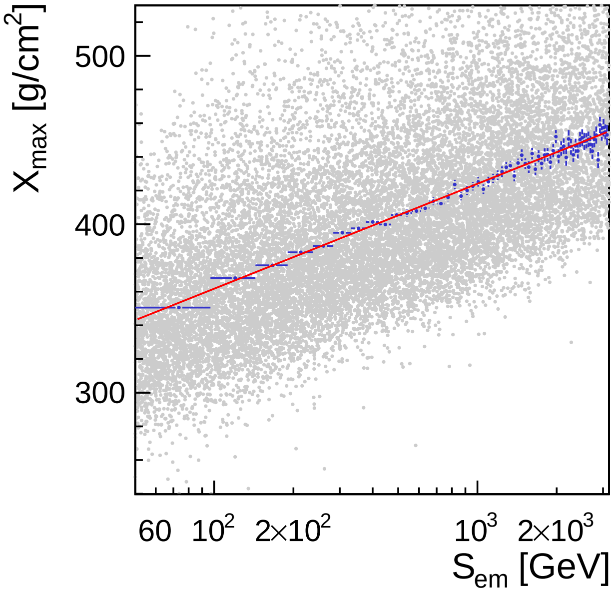

Figure 5. Correlation of the slant depth of the maximum of the air shower longitudinal profile, $X_{\rm max}$, with the energy deposited at the ground, $S_{\rm em}$.

where B_0 and γ_0 are parameters adjusted to describe the mean behaviour. The best parameterization is shown as the red curve with $B_0 = 237.1\,{\rm g\,cm^{-2}}$ and $\gamma_0 = 62.3\,{\rm g\,cm^{-2}}$.

Another, more precise estimation of $X_{\rm max}$ comes from looking at the shower front at the ground. The shower front is expected to form a curved surface [13] and this can be used to obtain X_{max}. An X_{max} that happens higher in the atmosphere will lead to a shower that is more open at the ground level since it had more time to interact and grow. The opposite happens when the X_{max} happens closer to the ground, and we have a tighter shower.

To explain how we can use the curvature to estimate X_{max}, we can imagine an ideal situation where the shower particles are produced in a single point established along the shower axis, which can be defined as the X_{max}. The surface of the shower front would then be a sphere since all the particles travel approximately at the speed of light. This means that the arrival time in each surface station would depend on the distance to the shower core and the primary particle direction. To reconstruct X_{max} we can use a simple geometrical fit, and the accuracy would primarily depend on the time resolution of the stations.

For a real-world situation, the geometry is more complex, but there is still a correlation between X_{max} and the arrival time distributions of particles at the ground. In Figure 6 we can see the time profile for an event with $X_{\mathrm{max}} = 339\,\mathrm{g\,cm^{-2}}$ and $E_0 = 1.3\,\mathrm{TeV}$. It was found that most of the events can be described by a quadratic polynomial of the form,

$$\Delta\mathrm{t}(\mathrm{r}) = a + b\,\boldsymbol{r} + c\,\boldsymbol{r}^2, \tag{3}$$

Applying this equation to the time profiles leads to a well behaved $\chi^2/n.d.f.$ distribution, with the distribution maximum peaking at ~ 1.2,

The parameter of the quadratic term of the polynomial, c, is strongly correlated with X_{max}, as seen in Figure 7. The parameter b is nearly independent of X_{max}, and a is associated with the event initial time, T_0, usually set to zero when the shower front reaches the shower core position.The dependence of c on X_{max} can be understood if one assumes that most of the particles produced in a shower come from X_{max} and the shower particles propagate as a spherical front. This is, of course, an approximation but Figure 7 supports it and it helps to build some intuition.

Hence, it is possible to parametrize X_{max} as a function of c using:

$$X^1_{\mathrm{max}} = B_1 + \gamma_1\, c. \tag{4}$$

with B_1 and γ_1 parameters set to describe the profile shown in Figure 7. The best achieved parametrization is shown by the red curve, with $B_1 = 11.2\,\mathrm{g\,cm^{-2}}$ and $\gamma_1 = 2.28 \times 10^9\ \mathrm{g\,s^{-1}}$.

As it can be seen in Figure 8, X^1_{max} does not have any relevant bias, even for low X_{max}. However, there are some cases, mainly at lower energies, where the number of particles arriving at the ground is small, the time profile fit may converge to c values that lead to non-physical values of X_{max}. This leads us to define that whenever the estimation of X_{max} from the equation (4) indicates values lower than $300\,\mathrm{g\,cm^{-2}}$, the first order estimation X^0_{max} is used. This value is decided due to the apparent divergence from the curve for X_{max} values of this order in Figure 7.

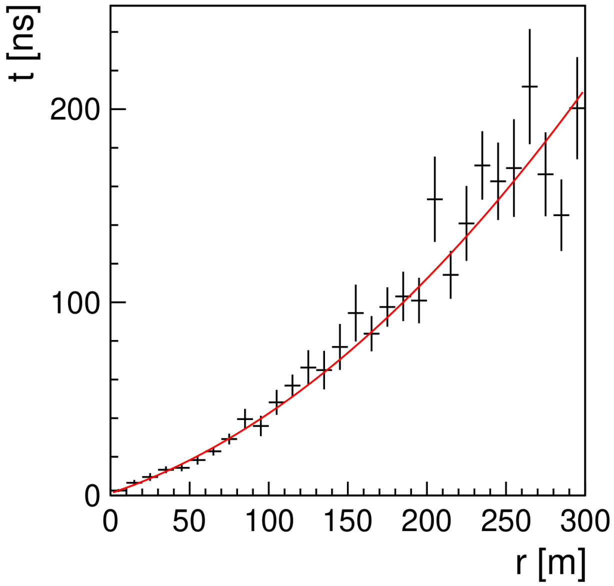

Figure 6. Arrival time as a function of the distance to the core for an event with $X_{\mathrm{max}} = 339\,\mathrm{g\,cm^{-2}}$ and $E_0 = 1.3\,\mathrm{TeV}$. The line correspond to a quadratic fit with its $\chi^2/\mathrm{ndf} = 0.93$.

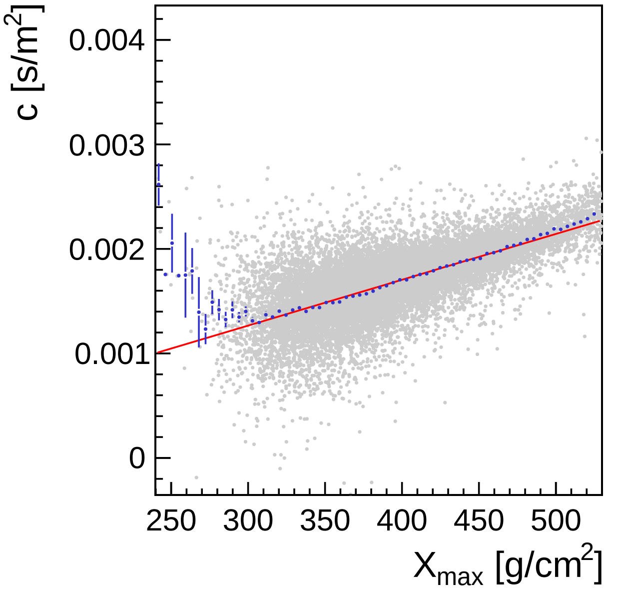

Figure 7. Correlation of the c curvature parameter with the slant depth of the maximum of the longitudinal profile, X_{max}.

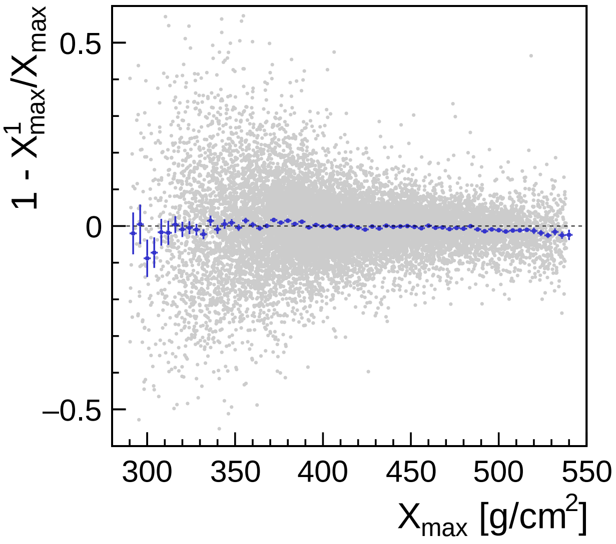

Figure 8. Normalized deviation of the estimator $X^1_{\rm max}$, defined in equation (4), from the real $X_{\rm max}$, as a function of $X_{\rm max}$.

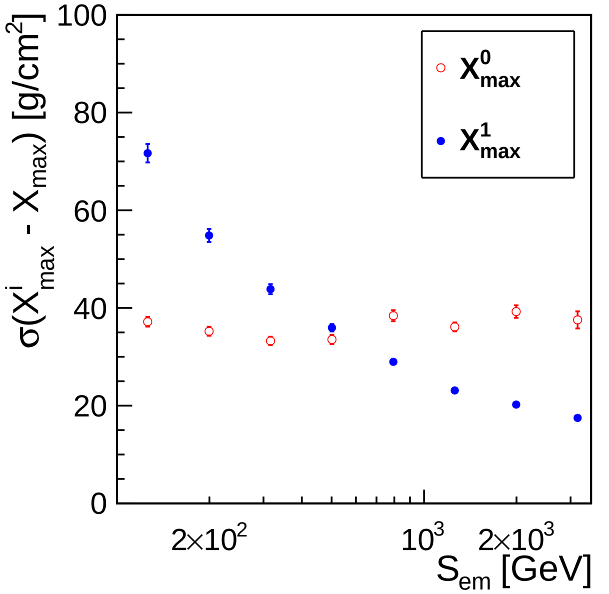

Figure 9. Resolution of the $X_{\rm max}$ estimators $X^0_{\rm max}$ and $X^1_{\rm max}$ as a function of $S_{\rm em}$.

The obtained resolutions as a function of $S_{\rm em}$, both for $X^0_{\rm max}$ and $X^1_{\rm max}$, are summarized in Figure 9. Resolutions of about $40\,{\rm g\,cm^{-2}}$ and $20\,{\rm g\,cm^{-2}}$ were found for primaries energies of 1 TeV and 10 TeV, respectively.

The resolutions for both $X^0_{\rm max}$ and $X^1_{\rm max}$ are similar in the region $S_{\rm em} \approx 400 - 600\,{\rm GeV}$. We can set the energy where the resolutions cross as $A_0^{\rm crX} = 600\,{\rm GeV}$, to be on the safe side, and avoid possible tail effects. Therefore, the estimator of $X_{\rm max}$, designated as $X^R_{\rm max}$ is defined as:

$$X^R_{\rm max} = \begin{cases} X^1_{\rm max} & \text{if } A_0 > A_0^{\rm crX} \\ & \text{and } X^1_{\rm max} > 300\,{\rm g\,cm^{-2}} \\ X^0_{\rm max} & \text{otherwise} \end{cases} \tag{5}$$

V. ENERGY RECONSTRUCTION AND RESOLUTION

The main idea behind this work is to improve the current energy reconstruction algorithms. This means we must define a benchmark for the reconstruction method so we can develop upon it. From now on we will call it the 0-order energy reconstruction. Most of the current experiments use a relation between the number of detector elements triggered, i.e., the energy measured at the ground, and the size of the shower to establish an estimate for the primary energy. The same idea will serve as the approach to define our 0-order reconstruction.

If we plot the logarithmic distribution of the energy lost in the atmosphere (E_0–$S_{\rm em}$), by the logarithmic of the electromagnetic energy deposited at the Earth surface, $S_{\rm em}$, we expect to see a linear correlation. This could immediately serve as a rough approach to the energy reconstruction. E_0 can be parameterized as a function of $S_{\rm em}$:

$$E_0^{(0)} = S_{\rm em} + C\,(S_{\rm em})^{\beta}, \tag{6}$$

with C and β free positive parameters.

The best parametrization is shown by the red line in Figure 10, and the values found for C and β are $37.2\,{\rm GeV}^{0.36}$ and 0.64, respectively.

We can then use this parametrization to get an estimate for the primary energy considering an ideal detector, that is, a detector that accurately collects all the energy of electromagnetic particles reaching the station. The energy resolution as a function of the primary energy for this method is shown in Figure 15 as the dotted line. As we can see, we obtained an energy resolution of about 35% for 1 TeV and a resolution of around 25% for 10 TeV. We have then established our 0-order for energy reconstruction.

Since we have established an estimator for $S_{\rm em}$, A_0, we can now do another reconstruction, using the same parametrization, but using A_0 instead. This way we obtain a result that would be more faithful to what could be obtained by an actual experiment, and it will help in the comparisons to the better energy reconstructions we will obtain.

Remembering the parametrization of equation 6, we have two free positive parameters, C and β, whose values have been obtained. The only difference is that now

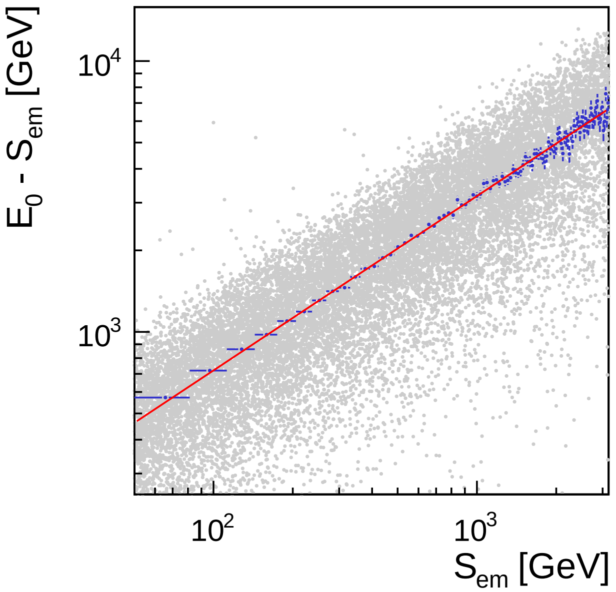

Figure 10. Correlation between the energy deposited in the atmosphere (primary energy minus the electromagnetic energy at the ground), $E_0 - S_{\rm em}$ and the energy deposited at the ground $S_{\rm em}$. The line corresponds to the best parametrization.

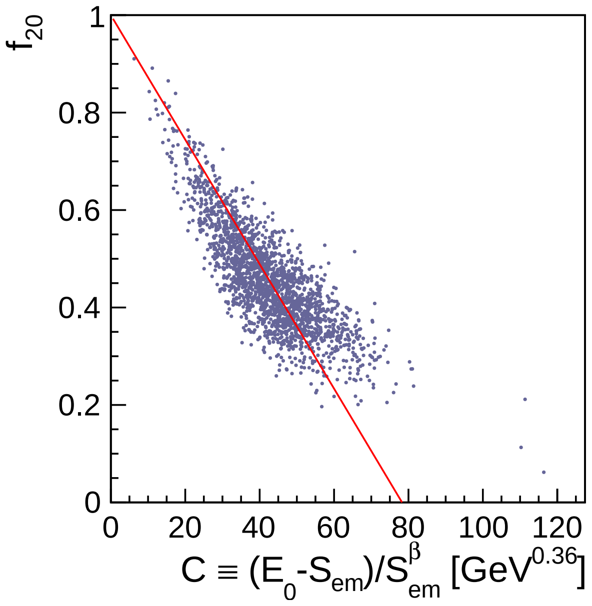

Figure 11. Correlation of the variable f_{20}, as defined in the text, with the calibration coefficient C, for events with $S_{\rm em} \sim 158\,{\rm GeV}$ and $X_{\rm max} \sim 358\,{\rm g/cm^2}$. The units on the x-axis come from the fact that C units are GeV/Gev$^{\beta}$ = GeV$^{(1-\beta)}$.

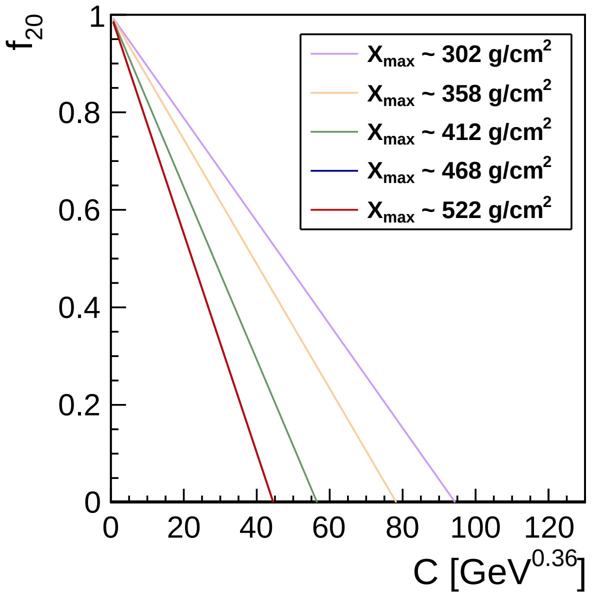

Figure 12. Calibration lines (f_{20}, C) for several ranges of $X_{\rm max}$ with $S_{\rm em} \sim 158\,{\rm GeV}$.

we will be using A_0 as a $S_{\rm em}$ estimator to obtain an energy reconstruction. In Figure 16 we have the energy resolution for this approach as the dotted line, and for 1 TeV we obtain a resolution of about 40%, whereas when using $S_{\rm em}$ we obtained a resolution of about 35%.

The coefficient C was defined as a constant for the benchmark approach to the energy reconstruction, but we have found that C can be correlated with f_{20}, $X_{\rm max}$ and $S_{\rm em}$. This means the parametrization of equation 6 will now become

$$E_0^{(1)} = S_{\rm em} + C(f_{20}, X_{\rm max}, S_{\rm em})\,(S_{\rm em})^{\beta}\,. \qquad (7)$$

For a given bin of $S_{\rm em}$ and $X_{\rm max}$, between f_{20} and $C = (E_0 - S_{\rm em})/(S_{\rm em})^{\beta}$ there is in fact a remarkable correlation. In Figure 11 we have that correlation for events with $S_{\rm em} \in [100; 250]\,{\rm GeV}$ and $X_{\rm max} \in [330; 385]\,{\rm g\,cm^{-2}}$.

The red line in Figure 11 is the best linear parameterization, with the assumption that when there was no energy deposited in the atmosphere, $C = 0$, all the energy at the ground was collected at a distance shorter than 20 m from the shower core position, $f_{20} = 1$.

The set of the correlation lines (f_{20}, C) for several $X_{\rm max}$ ranges and $S_{\rm em} \sim 200\,{\rm GeV}$, are shown in Figure 12. There is a linear monotonous decrease of the slope m of these lines with the increase of $X_{\rm max}$. In Figure 13 the obtained m are represented as a function of $X_{\rm max}$ for different bins of $S_{\rm em}$ together with the best linear parametrization for each $S_{\rm em}$ bin, which will be of the form $m = b_m + s_m\,X_{max}$.

Extrapolating the lines for $X_{\rm max} = 0$ we see that m will have a small positive value, that is non-physical. This means that this linear model is no longer valid for

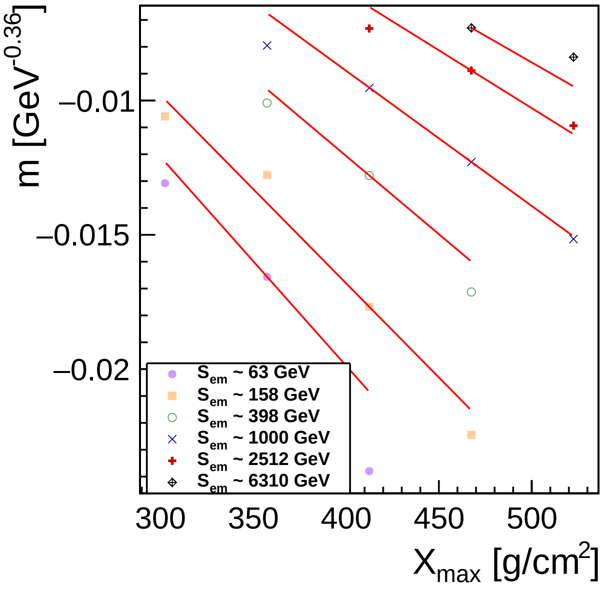

Figure 13. Correlation of the slope of the calibration lines, m, from with $X_{\max}$, for different S_{em} bins.

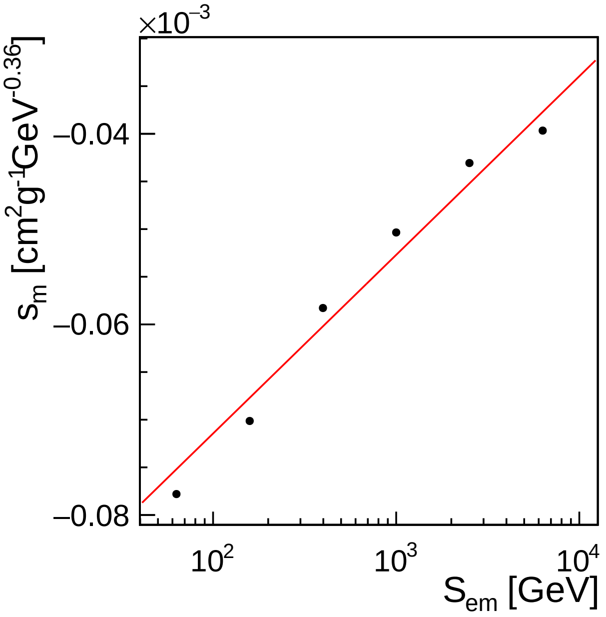

Figure 14. Correlation of the slope s_m of the m calibration lines represented in Figure 13 as a function of S_{em}.

$X_{\max} < 200\,\mathrm{g\,cm^{-2}}$, which is below the relevant region of $X_{\max}$ for this work. The b_m obtained for all S_{em} bins is around $0.011\,\mathrm{GeV}^{-0.36}$, so we will keep the linear approximation using this value.

In Figure 13 we can see that the slope, s_m, of the lines increases with S_{em}, so we plot s_m as a function of $\log(S_{\mathrm{em}})$ in Figure 14. In red we have the best parameterization, which is of the form $s_m = s_{m0} + s_{m1}\,\log(S_{\mathrm{em}}/\mathrm{GeV})$, with parameters $s_{m0} = -1.1 \times 10^{-4}\,\mathrm{GeV}^{-0.36}\,\mathrm{g}^{-1}\mathrm{cm}^2$ and $s_{m1} = 1.87 \times 10^{-5}\,\mathrm{GeV}^{-0.36}\,\mathrm{g}^{-1}\mathrm{cm}^2$. Putting it all together we have:

$$m(X_{\max}, S_{\mathrm{em}}) = b_m + [s_{m0} + s_{m1}\,\log(S_{\mathrm{em}}/\mathrm{GeV})]\,X_{\max}. \tag{8}$$

We can write f_{20} as:

$$f_{20} = 1 + m(X_{\max}, S_{\mathrm{em}})\,C(f_{20}, X_{\max}, S_{\mathrm{em}})\,. \tag{9}$$

These two equations together allow us to write C as

$$C(f_{20}, X_{\max}, S_{\mathrm{em}}) = \frac{1 - f_{20}}{-\left(b_m + [s_{m0} + s_{m1}\log(S_{\mathrm{em}})]\,X_{\max}\right)}\,. \tag{10}$$

We now finally have all the ingredients to write the new estimator of the primary energy, defined in equation 7.

To recapitulate, we now have two different energy reconstruction methods; a “real” simulated value of S_{em} and an estimation, A_0; and also, a “real” value for $X_{\max}$ and an estimator, $X^R_{\max}$, that is in itself two different types of estimation of $X_{\max}$. We can then try different combinations of these elements to obtain the definitive energy resolution.

Let us start by observing what happens when we use S_{em}. The 0-order reconstruction is shown in Figure 15 as the dotted line. The full lines correspond to $E_0^{(1)}$, with the thick line using the estimator of $X_{\max}$, and the thin line the real $X_{\max}$.

When using $X^R_{\max}$ an energy resolution of about 18 % and 12 % were obtained at 1 TeV and 10 TeV, respectively. Using the real $X_{\max}$ these energy resolutions improve to 8% and 4%. In fact, these results may be considered the *ultimate* resolutions, as they do not depend on the resolution of any other parameter.

Next, we can see the results when using A_0 as the estimator of S_{em} in Figure 16. The dotted line corresponds to the resolution obtained with a constant C coefficient, of about 40% for 1 TeV and around 30% for 10 TeV which we have defined earlier in this section. Again, the full lines correspond to $E_0^{(1)}$ with $X_{\max}$ and $X^R_{\max}$, but we have also added a dashed line that also uses $C(X_{\max}, f_{20})$ coefficient but with $X^0_{\max}$ for comparison.

Something of note is the effect of the resolution of A_0 in the energy resolution. A resolution of 12% on the parameter A_0, translates into a resolution on $E_0^{(1)}$, considering the simulated $X_{\max}$ value, of 22% for 1 TeV, while the so-called *ultimate* resolution was of only 8%. We can then ascertain that the resolution of the S_{em} estimator significantly restricts the energy resolution.

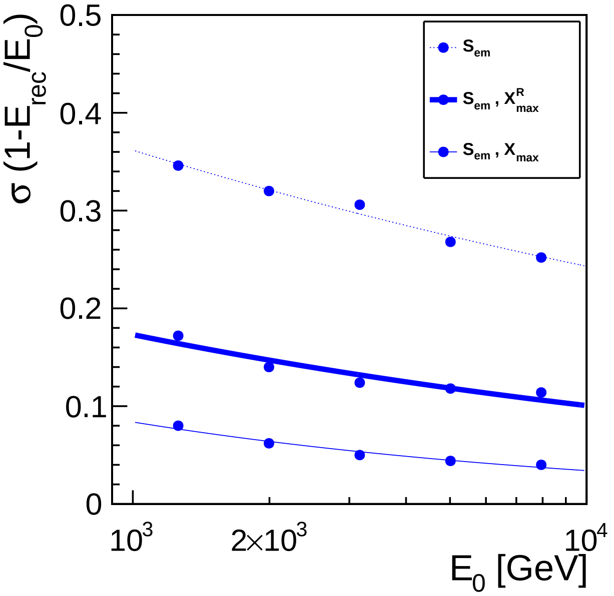

Figure 15. Energy resolution as a function of the primary energy, using $S_{\rm em}$. The dotted line corresponds to $E_0^{(0)}$, with constant C coefficient, (our benchmark). The full lines correspond to $E_0^{(1)}$, with $C(X_{\rm max}, f_{20})$ coefficient, using $X^R_{\rm max}$ (thick) or $X_{\rm max}$ (thin).

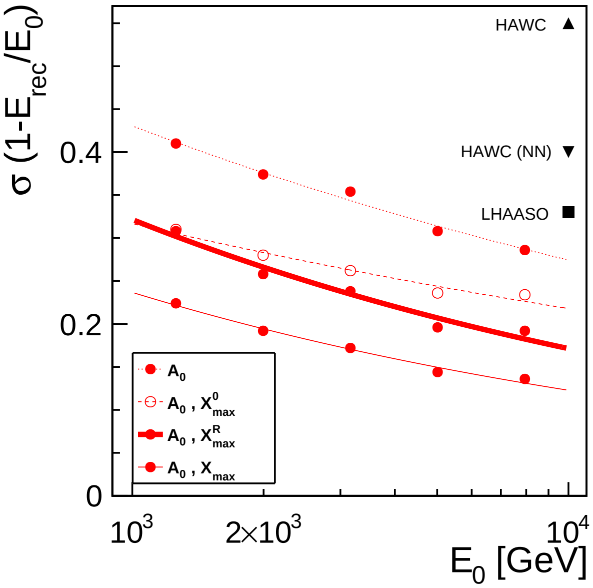

Figure 16. Energy resolution as a function of the primary energy, using A_0. The dotted line corresponds to $E_0^{(0)}$, with constant C coefficient. The full lines and the dashed line correspond to $E_0^{(1)}$, with $C(X_{\rm max}, f_{20})$ coefficient, using $X^R_{\rm max}$ (thick) or $X_{\rm max}$ (thin). The dashed line uses $X_{\rm max}$. For comparison the resolutions obtained for different experiments are also shown.

The impact of a flexible $X_{\rm max}$ reconstruction can also be gleaned by the difference of the energy resolution when using $X^R_{\rm max}$ and $X^0_{\rm max}$. While the energy resolution is about the same for lower energies, at around 30% for 1 TeV, as the primary energy increases we can see a reasonable improvement in the energy resolution for $X^R_{\rm max}$. At 10 TeV the obtained resolution is around 20%, whereas considering $X^0_{\rm max}$ we have a resolution of about 24%.

Ultimately, the closer energy reconstruction to a real-world scenario (although studying an ideal detector) would be the one we obtain with the estimated energy $E_0^{(1)}$ and the estimator of $S_{\rm em}$ and $X^R_{\rm max}$ (the thick full line in Figure 16). The energy resolution obtained this way is a significant improvement over the resolution obtained for our benchmarks, either considering the real or estimated $S_{\rm em}$.

VI. CONCLUSIONS

With this work, we have proposed new and innovative methods for the determination of the total electromagnetic energy at the ground, for the slant depth of the maximum of the longitudinal profile and the primary energy.

The obtained results, which have been published in [14], are very promising and can lead to new physics possibilities. The best-case real-world scenario for our energy reconstruction, with both $S_{\rm em}$ and $X_{\rm max}$ estimated, provides us with a resolution of around 20% for 10 TeV, which is a significant improvement over the resolutions currently provided by gamma-ray experiments, with HAWC standing between 40% (for a neural network based approach) and 55% [7] and LHAASO around 33% for the same energy [15]. These results are presented in Figure 16 for easier comparison. IACT typically have resolutions between 8% and 25% for 1 TeV and around 15% to 35% at 50 TeV [16–18], making our achieved resolutions comparable to what IACT can obtain.

The achieved results, which represent such a significant improvement over the currently quoted energy resolutions of existing or planned Wide Field of View Gamma-Ray Observatories, will undoubtedly motivate detailed simulations and studies on the applicability of the proposed methods.

---

[1] B. Rossi and K. Greisen, Cosmic-Ray Theory, Rev. Mod. Phys. **13**, 240 (1941).

[2] K. Greisen, Progress in cosmic ray physics **3** (1956).

[3] T. K. Gaisser and A. M. Hillas, Reliability of the Method of Constant Intensity Cuts for Reconstructing the Average Development of Vertical Showers, in *International Cosmic Ray Conference*, International Cosmic Ray Conference, Vol. 8 (1977) p. 353.

[4] J. Montanus, Intermediate models for longitudinal profiles of cosmic showers, Astropart. Phys. **35**, 651 (2012), arXiv:1106.1073 [astro-ph.HE].

[5] S. Andringa, R. Conceição, and M. Pimenta, Mass composition and cross-section from the shape of cosmic ray shower longitudinal profiles, Astroparticle Physics **34**, 360 (2011).

[6] G. Sciascio, Ground-based Gamma-Ray Astronomy: an Introduction, Journal of Physics: Conference Series **1263**, 012003 (2019).

[7] A. U. Abeysekara *et al.*, Measurement of the Crab Nebula Spectrum Past 100 TeV with HAWC, The Astrophysical Journal **881**, 134 (2019).

[8] D. Heck, J. Knapp, J. N. Capdevielle, G. Schatz, and T. Thouw, *CORSIKA: a Monte Carlo code to simulate extensive air showers.* (1998).

[9] T. T. Böhlen, F. Cerutti, M. P. W. Chin, A. Fassò, A. Ferrari, P. G. Ortega, A. Mairani, P. R. Sala, G. Smirnov, and V. Vlachoudis, The FLUKA Code: Developments and Challenges for High Energy and Medical Applications, Nucl. Data Sheets **120**, 211 (2014).

[10] A. Ferrari, P. R. Sala, A. Fasso, and J. Ranft, FLUKA: A multi-particle transport code (Program version 2005) (2005).

[11] S. Ostapchenko, Monte Carlo treatment of hadronic interactions in enhanced Pomeron scheme: I. QGSJET-II model, Phys. Rev. D **83**, 014018 (2011), arXiv:1010.1869 [hep-ph].

[12] In this work, the bias and resolutions of the estimator, $\hat{x}$, of variable, x, are taken fitting a gaussian function to the residuals, $(1 - (\hat{x}/x))$. The bias and the resolution corresponding to the mean and the sigma parameter of the fitted Gaussian, respectively.

[13] A. K. Calabrese Melcarne, G. Marsella, D. Martello, L. Perrone, and S. Sbano (ARGO-YBJ), Temporal and spatial structure of the extensive air shower front with the ARGO-YBJ experiment, in *32nd International Cosmic Ray Conference*, Vol. 1 (2011) pp. 66–69.

[14] R. Conceição, L. Peres, M. Pimenta, and B. Tomé, New methods to reconstruct X_{max} and the energy of gamma-ray air showers with high accuracy in large wide-field observatories, The European Physical Journal C **81**, 10.1140/epjc/s10052-021-08883-6 (2021).

[15] L. collaboration, Performance of LHAASO-WCDA and Observation of Crab Nebula as a Standard Candle (2021), arXiv:2101.03508 [astro-ph.IM].

[16] J. Aleksić *et al.*, Performance of the MAGIC stereo system obtained with Crab Nebula data, Astroparticle Physics **35**, 435 (2012), arXiv:1108.1477 [astro-ph.IM].

[17] R. D. Parsons and J. A. Hinton, A Monte Carlo template based analysis for air-Cherenkov arrays, Astroparticle Physics **56**, 26 (2014), arXiv:1403.2993 [astro-ph.IM].

[18] N. Park and VERITAS Collaboration, Performance of the VERITAS experiment, in *34th International Cosmic Ray Conference (ICRC2015)*, International Cosmic Ray Conference, Vol. 34 (2015) p. 771, arXiv:1508.07070 [astro-ph.IM].